NJC

Accepted Manuscript

This is an *Accepted Manuscript*, which has been through the Royal Society of Chemistry peer review process and has been accepted for publication.

Accepted Manuscripts are published online shortly after acceptance, before technical editing, formatting and proof reading. Using this free service, authors can make their results available to the community, in citable form, before we publish the edited article. We will replace this *Accepted Manuscript* with the edited and formatted *Advance Article* as soon as it is available.

You can find more information about *Accepted Manuscripts* in the Information for Authors.

Please note that technical editing may introduce minor changes to the text and/or graphics, which may alter content. The journal's standard Terms & Conditions and the Ethical guidelines still apply. In no event shall the Royal Society of Chemistry be held responsible for any errors or omissions in this *Accepted Manuscript* or any consequences arising from the use of any information it contains.

ROYAL SOCIETY OF CHEMISTRY

www.rsc.org/njc

Journal Name

RSCPublishing

ARTICLE

Synthesis and bactericidal evaluation of imide *N*-halamine-loaded PMMA nanoparticles

Cite this: DOI: 10.1039/x0xx00000x

Qigeqi Dong[a,b,1], Qian Cai[a,1], Yangyang Gao[a], Shiqi Zhang[c], Ge Gao[d], Chokto Harnoode[a], Morigen[b] and Alideertu Dong[a,*]

Received 00th January 2012,
Accepted 00th January 2012

DOI: 10.1039/x0xx00000x

www.rsc.org/

Imide *N*-halamine-loaded poly(methyl methacrylate) nanoparticles (PMMA) based on barbituric acid were synthesized as novel antimicrobial agents using the radical copolymerization. Evidence for loading imide *N*-halamine on PMMA nanoparticles has been inferred from different techniques like ^{1}H NMR, FTIR, TEM, SEM, and XPS analyses. Sterilizing effect of the products on bacterial strain was systematically evaluated by selecting *Staphylococcus aureus* (*S. aureus*), *Escherichia coli* (*E. coli*), and *Pseudomonas aeruginosa* (*P. aeruginosa*) as model pathogenic bacteria. The zone of inhibition study and the spread plate technique suggested that the imide *N*-halamine-loaded PMMA nanoparticles possessed powerful bactericidal activity towards both Gram-positive and Gram-negative bacteria. Effect of contact period, *N*-halamine structure, particle size, and chlorine content on biocidal efficiency were investigated as well. Long-term stability of the imide *N*-halamine-loaded PMMA nanoparticles was also confirmed as a function of storage period.

1. Introduction

Environment contamination induced by pathogenic microorganisms is of great concern in the medical field, public hygiene, food safety control, and water purification, etc[1,2]. Various kinds of bactericides thus have been prosperously developed in recent decades[3-6]. Of various bactericides, considerable research efforts have been devoted to fabricating *N*-halamines due to their instant and total sterilization of a wide range of microorganisms[7]. *N*-Halamines possess several overwhelming superiorities such as long-term storage, high stability, and regenerability[8]. Moreover, unlike inorganic halogens, *N*-halamines are durable, less corrosive, and do not decompose in water to form toxic products[9].

N-Halamines with one or more nitrogen-halogen covalent bond are generally synthesized through the halogenation of the corresponding amide, imide, or amino group[10]. 5,5-Dimethylhydantoin with one amide and one imide commonly accepted as *N*-halamine precursor has been widely reported. Worley et al. designed numerous *N*-halamines from 5,5-dimethylhydantoin with powerful antimicrobial activity against both Gram-positive and Gram-negative bacteria[11-13]. Sun et al. developed various kinds of *N*-halamine polymers from hydantoin-based monomer with outstanding antibacterial capability[14-16]. Liang's group loaded quaternarized *N*-halamine on cellulose showing excellent antimicrobial activity, washing durability, and storage stability[17-19]. Numerous studies have shown that the bactericidal activity of *N*-halamine is in an order of imide > amide > amine *N*-halamine[20]. Thereby, developing *N*-halamines with more imide structure to enhance antimicrobial efficiency is advisable. Barbituric acid famous for medical and biological function is promising heterocyclic compounds with two imide functional groups in the structure[21]. Imide group can readily transfer to N-Cl structure upon chlorination, by which imide type *N*-halamines as a potential biocide can be achieved. Nevertheless, reports corresponding to *N*-halamines based on barbituric acid are quite rare[22,23].

Antibacterial performance of *N*-halamines is strongly dependent on their surface area, and thus reducing materials' size to improve surface area is a promising idea[24]. Numerous reports confirmed that nanoparticles exhibit high antibacterial activity compared with their bulk counterparts owing to their larger activated surface area providing more active sites for deactivating pathogenic bacteria[25]. Selecting chemically inert nanoparticles with controllable size as solid supports to enhance the activated surface is most widely utilized. In our previous studies, several *N*-halamine antibacterial nanoparticles were prepared with silica, iron oxide, polystyrene, and poly(styrene-*co*-acrylic acid) nanoparticles as template, respectively[26-32]. Introduction of these templates can achieve the aim of improving the activated surface, but unavoidably bring about the fatal drawback that of the cumbersome synthesis procedures induced by more reacting steps and the pollution caused by the templates during the practical application. Afterwards, designing *N*-halamine nanoparticles without using solid templates was taken into account by our group, and the study for synthesizing *N*-halamine homopolymer nanoparticles via the radical polymerization of allyl monomer was thus carried out. Unfortunately, *N*-halamine homopolymers were hardly obtained because of the radical autoinhibition effect of allylic structure[33]. In response to such difficulty, methyl methacrylate favorable to radical polymerization was chosen to copolymerize with *N*-halamine monomer to obtain antibacterial polymer with higher molecular weight[34]. Few published studies concerned the preparation of functionalized PMMA nanoparticles through the one-step process by using the radical copolymerization of MMA with functional component[35,36].

General consideration, we report herein the facile synthesis of novel imide *N*-halamine nanoparticles as promising antibacterial agent through the functionalization of PMMA nanoparticles with barbituric acid-based *N*-halamine without using additional template

nanoparticles. Imide *N*-halamine-loaded PMMA nanoparticles were characterized with different techniques such as transmission electron microscopy (TEM), scanning electron microscopy (SEM), nuclear magnetic resonance (NMR), Fourier transform infrared (FTIR), and X-ray photoelectron spectra (XPS). To evaluate the bactericidal capability, *Staphylococcus aureus* (*S. aureus*, Gram-positive), *Escherichia coli* (*E. coli*, Gram-negative), and *Pseudomonas aeruginosa* (*P. aeruginosa*, Gram-negative) were selected as model bacteria. Antimicrobial results demonstrated that the as-synthesized imide *N*-halamine-loaded PMMA nanoparticles possessed excellent biocidal activity against both Gram-positive and Gram-negative bacteria.

2. Experimental section

2.1 Materials

Sodium and urea were obtained from Nanjing Chemical Reagent Co., Ltd. Anhydrous methanol, hydrochloric acid, hexane, tetrahydrofuran, diethyl ether, and acetone were purchased from Beijing Chemical Company. Methyl methacrylate and potassium persulfate were available from Tianjin Chemical Reagent Plant and Shanghai Chemical Reagent Plant, respectively. Sodium hydride was obtained from Beijing Hengye Zhongyuan Chemical Co., Ltd. Diethyl malonate, allyl bromide, magnesium sulfate, sodium chloride, sodium bicarbonate, and sodium hypochlorite were provided from Sinopharm Chemical Reagent Co., Ltd. The other reagents were analytical grade and were used without any purification.

2.2 Characterization

^{1}H NMR spectra were recorded on a Bruker AV300 instrument. FTIR spectra were captured by using a Thermo Nicolet (Woburn, MA) Avatar 370 FTIR spectrometer. TEM images were taken on a Hitachi H-8100 transmission electron microscope at 200 kV. X-ray photoelectron spectra (XPS) measurement was carried out on a PHI-5000CESCA system with Mg K radiation (hr = 1253.6 eV). The x-ray anode was run at 250 W, and the high voltage was kept at 14.0 kV with a detection angle at 540. All the binding energies were calibrated by using the containment carbon (C 1s = 284.6 eV). SEM images were taken on a Shimadzu SSX-550 field emission scanning electron microscope at 15.0 kV.

2.3 Preparation of 5-allylbarbituric acid

The suspension of 0.92 g sodium hydride in 50 mL tetrahydrofuran was added dropwise into 3.20 g diethyl malonate at 0 °C. The reaction mixture was warmed to room temperature and stirred for 1 h. Allyl bromide of 2.90 g was added, and the resulting solution was stirred overnight. After the addition of 100 mL ultrapure water and extraction with diethyl ether, the organic layer was washed with brine, dried with magnesium sulfate and concentrated under reduced pressure. The crude product was purified by column chromatography (hexane/diethyl ether, 10:1) to afford 3.44 g diethyl allylmalonate. A mixture of dry sodium methoxide [prepared from 0.2875 g sodium and 7.5 mL methanol], 0.75 g urea, 2.5 g diethyl allylamlonate, and 2.5 mL acetone was stirred under reflux for 7 h. The precipitate was collected by filtration, washed with acetone, suspended in 5 mL water, and acidified with concentrated aqueous hydrochloric acid to pH 1-2. The precipitate was filtered off and recrystallized from ethanol to obtain 5-allylbarbituric acid (ABBA) as colorless needles[37,38].

2.4 Preparation of poly(ABBA-*co*-MMA) nanoparticles

Sodium bicarbonate, potassium persulfate, and 100 mL ultrapure water were added in a 250 mL three-necked flask with a condenser and a N_2 gas inlet, and a mixture of ABBA dissolved in methyl methacrylate was added. The reaction mixture was maintained at 75 ^{o}C with stirring for 24 h. Copolymer nanoparticles with different particle sizes (523.81 nm, 809.52 nm, 904.76 nm, and 976.19 nm) were fabricated at different monomer concentration (1.0 wt %, 2.0 wt %, 3.0 wt %, and 5.0 wt %).

2.5 Preparation of imide *N*-halamine-loaded PMMA nanoparticles

Poly(ABBA-*co*-MMA) nanoparticles were immersed in a 10 % commercial aqueous sodium hypochlorite solution buffered at pH 7 at room temperature for 12 h. The imide *N*-halamine-loaded PMMA nanoparticles were washed thoroughly with ultrapure water and dried at 40 ^{o}C for 6 h to remove any remaining free chlorine from the surface of the sample[16-18].

2.6 Determination of chlorine content

Active chlorine content of the imide *N*-halamine-loaded PMMA nanoparticles was determined by the iodometric/thiosulfate titration procedure[9-16]. The weight percentage of chlorine (Cl %) for the sample was calculated according to the following equation[9,16].

$$Cl\% = \frac{35.5}{2} \times \frac{(V_{Cl} - V_0) \times 10^{-3} \times 0.01}{W_{Cl}} \times 100$$

where V_{Cl} and V_0 are the volumes (mL) of sodium thiosulfate solutions consumed in the titration of the chlorinated and unchlorinated samples, respectively, and W_{Cl} is the weight of the chlorinated sample (g).

2.7 Antibacterial test

The antibacterial behavior of the product was assessed by a modified Kirby-Bauer (KB) technique[39]. The surface of Luria Bertani agar plate and tryptic soy agar plate was overlaid with 1 mL of 10^{8-9} CFU/mL of *E. coli* (ATCC 8099, Gram-negative bacteria). The plates were then allowed to stand at 37 ^{o}C for 4 h. The imide *N*-halamine-loaded PMMA nanoparticles was placed onto the surface of each of the bacteria-containing agar plate, and gently pressed with a sterile forceps to ensure full contact between the sample and the agar. The same procedure was also applied to the pure PMMA nanoparticles as control. After incubation at 37 ^{o}C for 24 h, the inhibition zone around the sample was measured.

S. aureus (ATCC 25923, Gram-positive bacteria) and *P. aeruginosa* (ATCC 27853, Gram-negative bacteria) were used as model microorganisms to test the antibacterial activities of the samples. Bacteria were grown overnight at 37 °C in Luria-Bertani medium (LB, 10 g of tryptone and 5 g of yeast extract/liter). Cells were harvested by centrifugation, washed twice with phosphate-buffered saline (PBS, NaCl, 8.0 g/L; KCl, 0.20 g/L; $Na_2HPO_4 \cdot 12H_2O$, 3.49 g/L; KH_2PO_4, 0.2 g/L; pH 7.4), and diluted to concentrations of 10^{6-7} colony-forming units/mL. 100 mg of each sample was dispersed in 0.45 mL sterilized distilled water, vortexed, and then sonicated for 30 min. In antibacterial test, 50 µL of bacteria suspension and 450 µL of sample suspension were well mixed, and the mixture was incubated under constant shaking. After a certain period of contact time, 4.5 mL of 0.03 wt % sodium thiosulfate aqueous solution, sterilized by passing through 0.22 µm membrane and exhibited no effect on the growth of bacteria, was added into the reaction suspension to neutralize the active chlorine and stop the antibacterial action of sample. The resulting mixture was mixed well, serially diluted, and then 100 µL of each dilution was dispersed onto LB agar plates. Colonies on the plates were counted after incubation at 37 ^{o}C for 24 h.

3. Results and discussion

3.1 Characterization of poly(ABBA-*co*-MMA) nanoparticles

The fabrication of imide *N-halamine*-loaded PMMA nanoparticles mainly involves three steps, and each step is well controllable. As shown in Scheme 1, 5-allylbarbituric acid was synthesized from diethyl malonate by the cyclization reaction between urea and

diethyl allylmalonate, and copolymerized subsequently with methyl methacrylate via the radical polymerization followed by chlorination. ^{1}H NMR spectra of ABBA, MMA, and poly(ABBA-*co*-MMA) are illustrated in Fig. 1. The measurement was carried out by the aid of DMSO solvent, and the corresponding fitting signal for DMSO was detected at δ = 2.5 ppm, which is obviously observed in all these three spectra[40]. The assignments of the signals in ABBA are δ = 2.8, 3.7, 5.1, and 5.6 ppm, respectively in Fig. 1A. In the spectrum of MMA (Fig. 1B), the CH_2=C group shows signals at δ = 5.8 ppm and 6.0 ppm, and the C-CH_3 and O-CH_3 displayed the resonance peak at δ = 3.8 ppm and 1.8 ppm, respectively. After copolymerization, CH-, CH_2-, and CH_3- signal for poly(ABBA-*co*-MMA) were clearly observed in Fig. 1C[41,42], whereas the CH_2=C signals of ABBA and MMA component can no longer be detected. The corresponding peaks in the ^{1}H NMR spectra reflected the successful formation of poly(ABBA-*co*-MMA) via the radical copolymerization of ABBA with MMA. Introducing MMA as comonomer can not only avoid skillfully the autoinhibition effect of ABBA but also enhance the reactivity of ABBA towards chain propagation reaction.

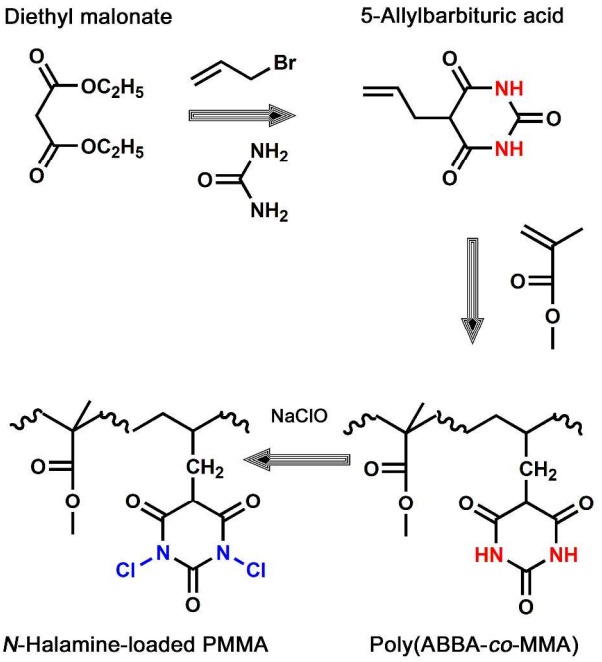

Scheme 1 Synthetic procedure of the imide *N*-halamine-loaded PMMA nanoparticles based on 5-allylbarbituric acid.

FTIR analysis was also performed to further confirm the existence of the functional groups of different samples. Fig. 2 exhibits FTIR spectrum of ABBA (A), MMA (B), and poly(ABBA-*co*-MMA) (C). The peaks at around 2985, 2926, and 1435 cm^{-1} are assigned to the stretching vibration and bending vibration of C-H bond, respectively[43]. The characteristic strong peak at around 1726 cm^{-1} is corresponding to the vibration of C=O band[44]. These peaks mentioned above are observed in all three curves. In Fig. 2A, the peak at 1248 cm^{-1} is corresponding to the C-N stretching vibration, and N-H stretching peak is appeared at 3200-3400 cm^{-1} [45]. The band at 1639 cm^{-1} refers to the stretching mode of C=C band[46]. In Fig. 2B, besides the C=C band, the peak at 1093 cm^{-1} is attributed to C-O-C stretching vibration[47]. After copolymerization, the characteristic peaks corresponding to C-N, N-H, C-O-C band were also observed for poly(ABBA-*co*-MMA) in Fig. 2C, while the C=C stretching peak disappeared at 1639 cm^{-1}, further demonstrating the fracture of the C=C bond during the radical copolymerization.

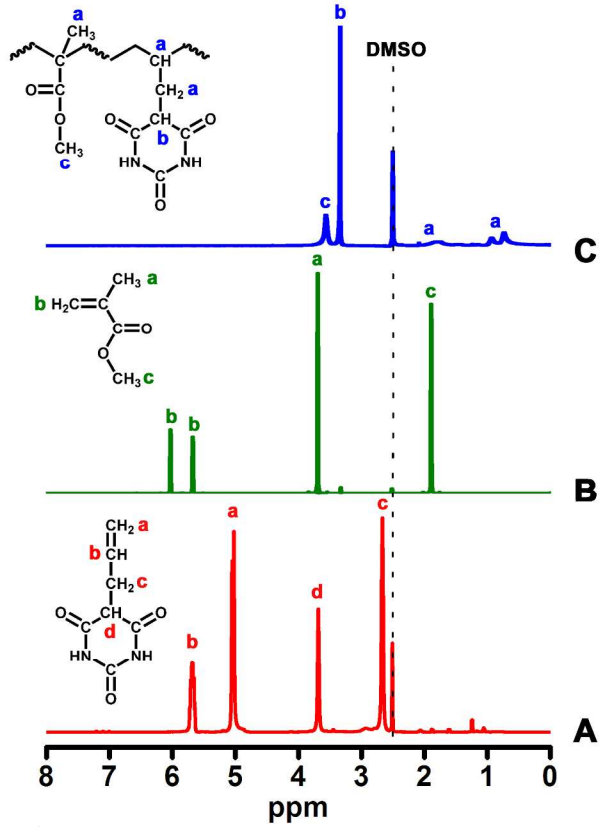

Fig. 1 ^{1}H NMR spectrum of ABBA (A), MMA (B), and poly(ABBA-co-MMA) (C).

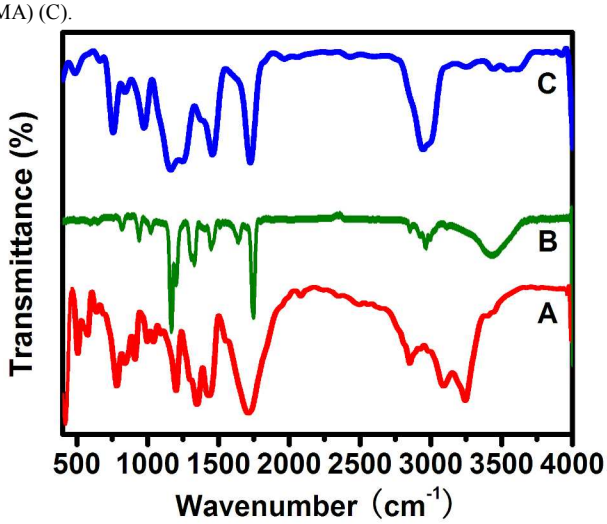

Fig. 2 FTIR spectrum of ABBA (A), MMA (B), and poly(ABBA-*co*-MMA) (C).

3.2 Characterization of imide *N*-halamine-loaded PMMA nanoparticles

The fabrication of imide *N*-halamine-loaded PMMA nanoparticles accomplished by chlorination of poly(ABBA-*co*-MMA) nanoparticles. TEM acts as an effective tool for microstructure characterization was carried out to investigate the morphology, structure, surface state, and particle size of the products[48]. Fig. 3A presents the typical TEM images of the imide *N*-halamine-loaded PMMA nanoparticles. Except a tiny minority with conglutinate and tortuous, most nanoparticles are uniform, quasi-monodisperse, spherical, smooth, and solid. The particle sizes are in a narrow range of 470-600 nm with an average size of ~522 nm. The magnified TEM image of the imide *N*-halamine-loaded PMMA nanoparticles is

given in the insert of Fig. 3A to further verify the surface state, showing flawless surface without any cracks or degradation. To substantiate the impact caused by the introduction of *N*-halamine on microstructure, pure PMMA nanoparticles with similar diameter were also synthesized by the radical polymerization and characterized by TEM as shown in Fig. 3B. No significant difference is observed in microstructure between pure PMMA and their *N*-halamine decorated counterparts. This phenomenon commendably reveals that the morphology, structure, and surface state of the as-synthesized nanoparticles were not influenced by introducing the *N*-halamine component.

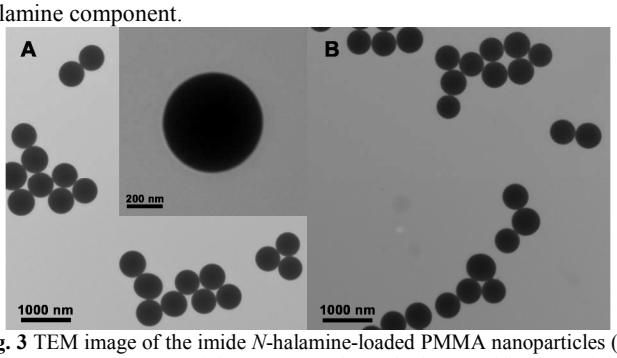

Fig. 3 TEM image of the imide *N*-halamine-loaded PMMA nanoparticles (A) and pure PMMA nanoparticles (B). Insert in 3A is the magnified TEM image of the imide *N*-halamine-loaded PMMA nanoparticles.

Detailed information about the chemical composition of the poly(ABBA-*co*-MMA) nanoparticles before and after chlorination was provided by XPS measurement as shown in Fig. 4. XPS is always introduced to assess the surface composition, and the detection depth for inorganic materials is about 2 nm and less than 10 nm for organic materials[49]. The characteristic peaks assigned to photoelectrons originating from the C 1s, N 1s, and O 1s energy level appear for both two samples at 285, 400, and 533 eV, respectively, which act as the signal markers for the ABBA and MMA components[50]. In particular, the presence of N 1s characteristic peak magnified in the insert image further reflects the successful immobilization of barbituric acid group on PMMA nanoparticles. Significant difference of Cl 2p peak between poly(ABBA-*co*-MMA) (Fig. 4A) and imide *N*-halamine-loaded PMMA nanoparticles (Fig. 4C) is clearly seen from the magnified insert images, suggesting the formation of N-Cl bond after chlorination treatment. Two weak peaks corresponding to the photoelectrons from Si 2s and Si 2p energy level are obtained at 154 and 103 eV possibly from the Si substrate used for sample immobilization[51]. For further clarification, the chemical bonds of the samples are identified by deconvolution of the C 1s peak from the total XPS spectrum. All chemical bonds referred to C element can be captured by the deconvolution of C 1s peak. One can see that both two peaks fitting of C 1s (Fig. 4B and Fig. 4D) has been curved into C-C, C-N, C-O, and C=O peak components[52]. It is quite reasonable to conclude from the C-O and C-N peak that MMA and ABBA exist either at or very near the particle surface. Generally, the presence of C 1s, O 1s, N 1s, and Cl 2p spectrum not only exhibits the surface chemistry but also confirms the formation of imide *N*-halamine-loaded PMMA nanoparticles.

3.3 Antimicrobial assessment

The N-H structure can be transformed facilely into N-Cl group upon treatment with sodium hypochlorite to obtain the target *N*-halamine product[53]. The as-synthesized products can be utilized as bactericides for treating microorganism as schematically illustrated in Scheme 2. In this study, the poly(ABBA-*co*-MMA) nanoparticles were immersed in sodium hypochlorite solution, and the chlorine content of the as-synthesized imide *N*-halamine-loaded PMMA nanoparticles was determined by the aid of iodometric/thiosulfate titration method[54]. It can be expected that imide *N*-halamine-loaded PMMA nanoparticles have potent antibacterial capabilities originated from *N*-halamine component. Zone of inhibition study is one effective approach for determining the antimicrobial behavior of the biocides[55]. It is well accepted that zone of inhibition is proportionate to their bactericidal activity. The larger the diameter of inhibition zone (DIZ) is, the more active it will be. Herein, DIZ value referred to the imide *N*-halamine-loaded PMMA nanoparticles was assessed using *E. coli* as the representative microorganism by a disk diffusion test. For comparison, the DIZ value of pure PMMA as comparative was estimated as well. The control experiments have a robust growth of bacteria. Pure PMMA nanoparticles do not show any inhibition zone, indicating that the support component is not toxic to the bacteria. Unlike pure PMMA, the imide *N*-halamine-loaded PMMA nanoparticles show a palpable inhibition ring size of 5.6 mm, indicating significant antibacterial activity against *E. coli*. Accordingly, it is considered that the excellent biocidal function of the imide *N*-halamine-loaded PMMA nanoparticles is provided completely by the *N*-halamine component.

The antibacterial performance of the imide *N*-halamine-loaded PMMA nanoparticles was further examined against *P. aeruginosa* by using the spread plate technique[56]. Similarly, the antibacterial assay of the pure PMMA nanoparticles was carried out comparatively by the same method. No significant difference is found between the control and PMMA nanoparticles, whereas obvious decrease is detected in the population of the bacterial colonies after the exposure to the imide *N*-halamine-loaded PMMA nanoparticles. The fact is in good agreement with the DIZ results. The excellent disinfection behavior of the imide *N*-halamine-loaded PMMA nanoparticles based on barbituric acid makes them the promising candidates for deactivating bacteria or even disease control.

3.4 Effect of contact period

The antimicrobial kinetic test confirmed the effect of contact time on the biocidal capability of imide *N*-halamine-loaded PMMA nanoparticles. The antibacterial kinetic curves, shown in Fig. 5, present the biocidal activity of pristine PMMA and their imide *N*-halamine-loaded counterparts by selecting both *P. aeruginosa* and *S. aureus*. The number of the survival bacterial colonies was counted as a function of the contact time ranged from 0 min to 60 min. As expected, PMMA nanoparticles almost show horizontal development trend, whereas significant bacterial reduction is observed upon the exposure to imide *N*-halamine-loaded counterparts both *P. aeruginosa* and *S. aureus* for the whole contact time range. A sharp increasing trend in bacterial reduction is observed within the lower contact time range, and bactericidal speed slows down gradually as extending exposure period, which suggests that the imide *N*-halamine-loaded PMMA nanoparticles are more suitable for fast sterilization[18,30,57]. The antibacterial results also indicated that the imide *N*-halamine-loaded PMMA nanoparticles have different capability towards *P. aeruginosa* and *S. aureus*. As a general observation, the products provided faster antibacterial action against *P. aeruginosa* than *S. aureus* within the same contact time. Therefore, it can be considered that *P. aeruginosa* would be more vulnerable than *S. aureus* towards the *N*-halamine-based antibacterial agents. This phenomenon may be attributed to the different cell structures of *P. aeruginosa* and *S. aureus*[58].

Journal Name RSCPublishing

ARTICLE

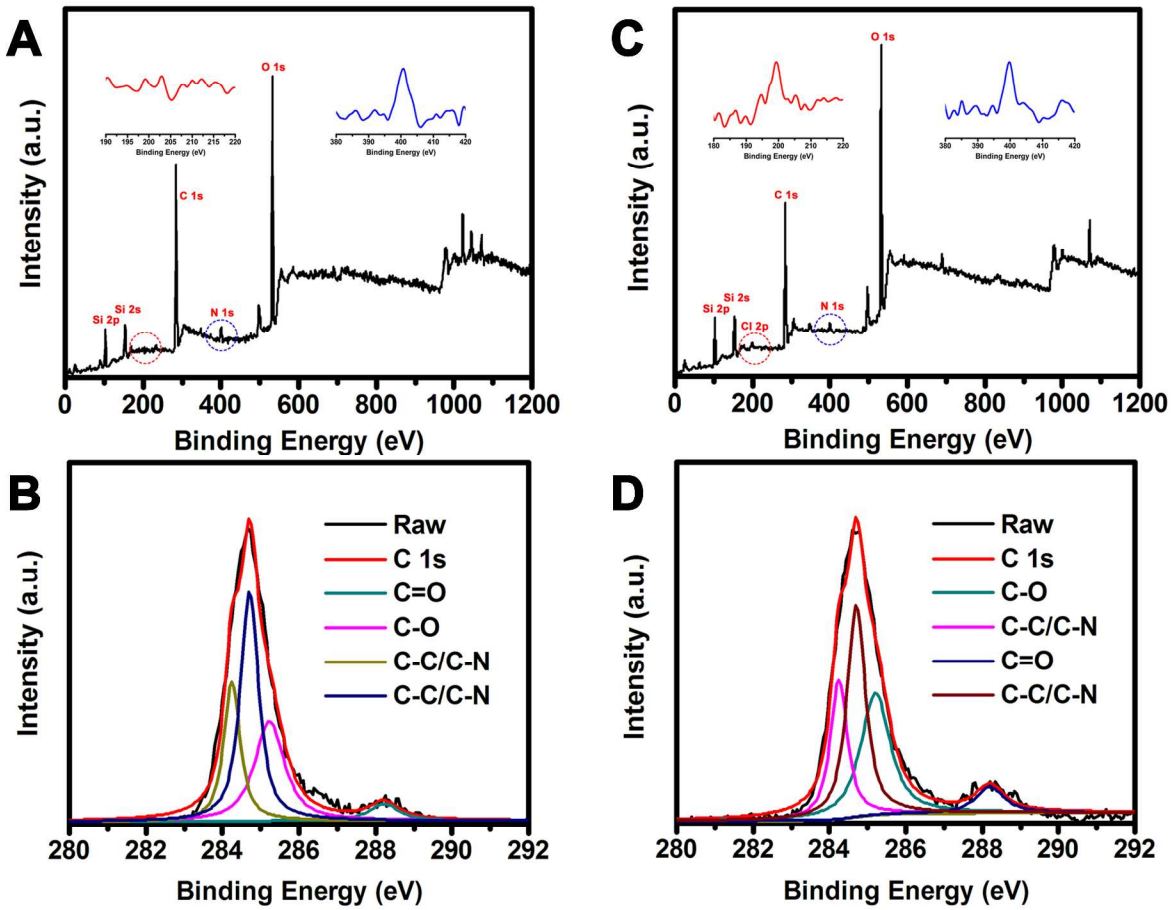

Fig. 4 XPS survey (A and C) and C 1s (B and D) spectrum of poly(ABBA-*co*-MMA) (A and B) and imide *N*-halamine-loaded PMMA nanoparticles (C and D).

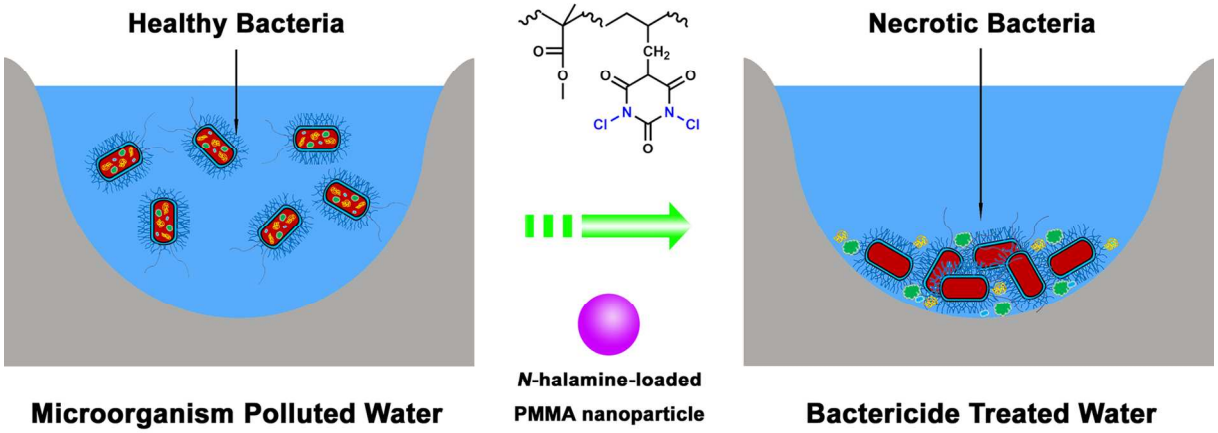

Scheme 2 Picture showing microorganism treated with the imide *N*-halamine-loaded PMMA nanoparticles.

Journal Name RSCPublishing

ARTICLE

3.5 Effect of *N*-halamine structure

It is acknowledged that the bactericidal activity of *N*-halamine is in the order of imide > amide > amine. In our previous reports, we designed several hydantoin-based *N*-halamine nanoparticles and their antimicrobial behavior was studied systematically. Hydantoins contain one imide and one amide group in structure, while barbituric acid is heterocyclic compound with two imide groups. Therefore, it is reasonable to consider that barbituric acid-type *N*-halamine would be more effective than hydantoin-based *N*-halamine for deactivating bacteria. To substantiate the hypothesis, the bactericidal capability of barbituric acid-originated *N*-halamine nanoparticles was quantitatively compared with hydantoin-structural *N*-halamine nanoparticles via the test of minimum inhibitory concentration (MIC). MIC was defined as the sample concentration at which the colonies were reduced in the CFU/mL numbers of ≥3 log[59]. Herein, the MIC value of the samples against *S. aureus* and *P. aeruginosa* was determined by the agar plate method as shown in Fig. 6. The MIC value of barbituric acid-based *N*-halamine nanoparticles against *S. aureus* and *P. aeruginosa* are 40 and 20 mg/mL, respectively, and 80 and 80 mg/mL for hydantoin-based *N*-halamine nanoparticles. It is well known that MIC value of the biocides reflects the magnitude of the susceptibility to the bacteria, and the antibacterial capability is inversely proportional to the MIC value. Thereby, the antibacterial efficiency of barbituric acid-based *N*-halamine nanoparticles is higher than that of hydantoin-based counterparts. This phenomenon is attributed to the structure difference between barbituric acid-based and hydantoin-originated *N*-halamine[30,32].

3.6 Effect of particle size

As for *N*-halamines, the particle size is a decisive parameter determining the bactericidal capability. The antimicrobial efficiency can be enhanced by reducing the particle size because the expanded surface area provides more activated surface sites that can kill the bacteria. To confirm the size effect, the imide *N*-halamine-loaded PMMA nanoparticles with different particle sizes (523.81 nm, 809.52 nm, 904.76 nm, and 976.19 nm) were prepared and characterized by TEM technique. Fig. 7 illustrates the representative SEM image of imide *N*-halamine-loaded PMMA nanoparticles with different diameters. Except particle size, morphology, structure, and surface state have shown no distinguishable difference among them.

Normally, the particle size is inversely proportional to the surface area. The corresponding surface area of the products with different size was calculated based on the assumption that the nanoparticles are non-porous spheres with density of 1.0 $g \cdot cm^{-3}$. The calculation was performed according to the following equation: $S = 6(D \cdot d)^{-1}$, wherein S is the surface area ($m^2 \cdot g^{-1}$); D is the diameter (μm); and d is the density ($g \cdot cm^{-3}$) of the sample[60]. The antimicrobial efficiency of the imide *N*-halamine-loaded PMMA nanoparticles with different size against *S. aureus* was determined comparatively. Table 1 summarizes the trend of bactericidal activity correlated to particle size and surface area within the same contact time of 60 min. Nanoparticles with particle size of 523.81 nm/surface area of 11.45 $m^2 \cdot g^{-1}$ show as high as 95.63 % colonial reduction, and the antimicrobial efficiency decreases with increasing particle size/decreasing surface area, even 976.19 nm/6.15 $m^2 \cdot g^{-1}$ nanoparticles can only kill 55.12 % *S. aureus*. In general, the imide *N*-halamine-loaded PMMA nanoparticles with smaller size/higher surface area reveal stronger bactericidal capability towards bacterial colonies. The performance of the imide *N*-halamine-loaded PMMA nanoparticles with different diameter proves the size effect hypothesis.

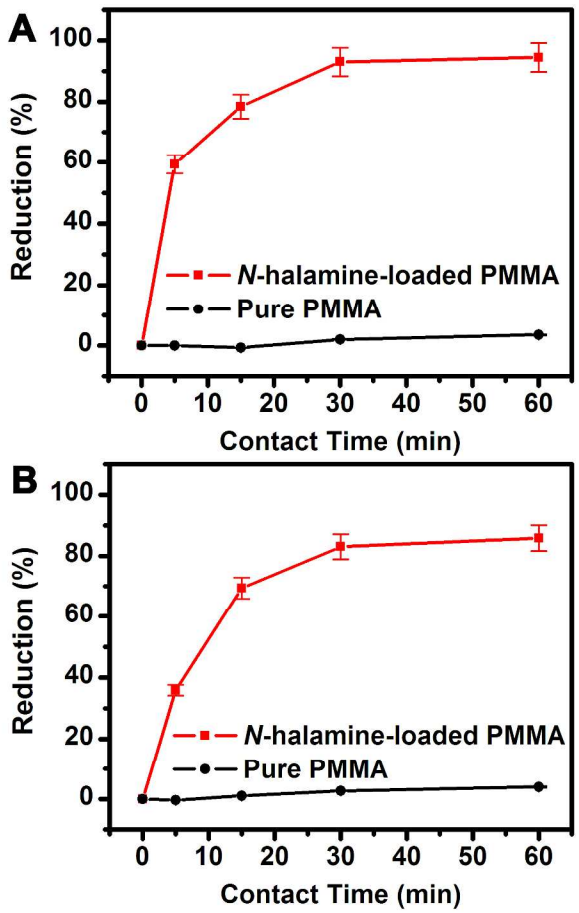

Fig. 5 Antibacterial kinetic test graphs for pure PMMA and the imide *N*-halamine-loaded PMMA nanoparticles against *P. aeruginosa* (A) and *S. aureus* (B).

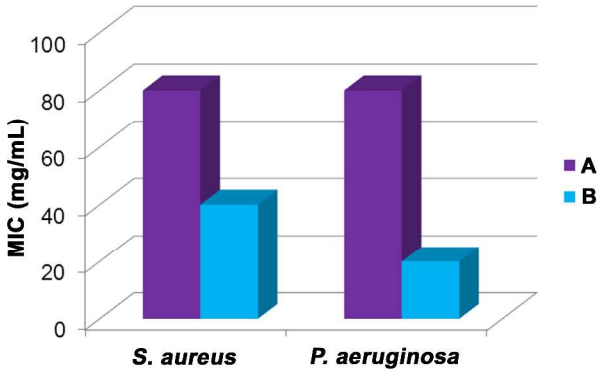

Fig. 6 Minimum inhibitory concentration (MIC) of hydantoin-originated (A) and barbituric acid-based (B) imide *N*-halamine-loaded PMMA nanoparticles towards *S. aureus* and *P. aeruginosa*.

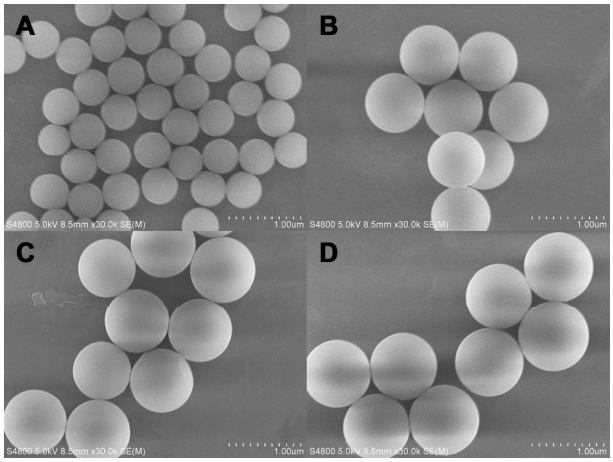

Fig. 7 SEM image of the imide *N*-halamine-loaded PMMA nanoparticles with different particle size.

Table 1 Reduction of bacterial colonies (*S. aureus*) after the 60 min exposure to the imide *N*-halamine-loaded PMMA nanoparticles with different particle size and activated surface area.

Sample	Size (nm)	Surface Area ($m^2 \cdot g^{-1}$)	Reduction (%)
S1	523.81	11.45	95.63
S2	809.52	7.41	80.37
S3	904.76	6.63	73.36
S4	976.19	6.15	55.12

3.7 Effect of chlorine content

Chlorine content also plays an important role in governing the antibacterial activity of *N*-halamines[61]. The relationship between the chlorine content and biocidal activity is constructed by means of *S. aureus* reduction as a function of chlorine content as shown in Fig. 8. In general, bacterial reduction displays upward trend with the increasing chlorine loading. Merely 51 % *S. aureus* reduction is observed for the 0.07 Cl % sample, while as high as 95 % reduction for 0.61 Cl % sample after 60 min contact with the biocides. Consequently, it is irrefutable that the antimicrobial capability of *N*-halamines is proportional to chlorine content, because the product with higher chlorine loading can offer more activated sites, resulting in the enhanced antibacterial efficiency. Interestingly, bacterial colonies reduce drastically with increasing chlorine content within the lower chlorine content region, and then level off with extending chlorine loading. The most probable reason is detailed as follows. Although increased chlorine content usually leads to enhanced bactericidal efficacy, it can also render the surface more hydrophobicity, resulting in poorer contact with the bacteria and thus less efficacy. Generally, bacterial reduction trend shows dramatic increase firstly and calm down with increasing chlorine content.

3.8 Stability test

The practical application of the biocides is always dependent on their stability. Long-term stability is a distinguishable feature of *N*-halamine-based biocidal agents[62]. In order to verify the stability, the imide *N*-halamine-based PMMA nanoparticles with 0.61 % chlorine content were stored at about 25 ^{o}C and 50 % RH for one month, and after that, the remaining chlorine was measured by the iodometric/thiosulfate titration. Interestingly, there is no visible reduction in the chlorine content after one month storage, indicating that the imide *N*-halamine-loaded PMMA nanoparticles possess quite higher stability in the dry state. Thanks to these overwhelming advantages, the as-synthesized imide *N*-halamine-loaded PMMA nanoparticles are promising antimicrobial agents for various fields.

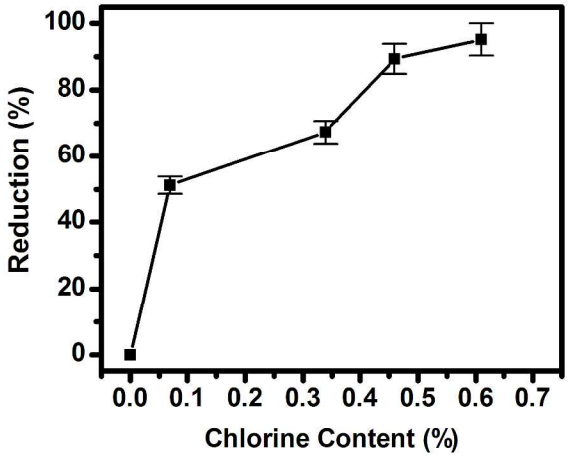

Fig. 8 Reduction of bacterial colonies (*S. aureus*) after the 60 min exposure to the imide *N*-halamine-loaded PMMA nanoparticles with different chlorine content.

4. Conclusions

We developed an efficient approach for the design and synthesis of the imide *N*-halamine-loaded poly(methyl methacrylate) nanoparticles based on barbituric acid by the radical copolymerization. The as-synthesized products were well characterized by 1H NMR, FTIR, TEM, SEM, and XPS analyses, and exhibited excellent bactericidal capability both against Gram-positive and Gram-negative bacteria. Contrast test illustrated that poly(methyl methacrylate) supports have no biocidal activity at all, and the antimicrobial activity of the imide *N*-halamine-loaded poly(methyl methacrylate) nanoparticles arises from imide *N*-halamine. The antimicrobial kinetic test confirmed the effect of contact time on the biocidal capability of imide *N*-halamine-loaded poly(methyl methacrylate) nanoparticles. Structural effect of *N*-halamine on biocidal efficiency was justified by the comparison between barbituric acid-based and hydantoin-based *N*-halamine. Bactericidal capability of the imide *N*-halamine-loaded poly(methyl methacrylate) nanoparticles with different particle sizes and different chlorine contents was studied systematically as well. After long-term storage, the imide *N*-halamine-loaded poly(methyl methacrylate) nanoparticles showed excellent stability in the dry state. We believe that the present study opens up the possibility for extensive investigation of the antimicrobial *N*-halamines, broading their practical applications in various fields.

Acknowledgements

This research was supported by the National Natural Science Foundation of China (21304044) and the Supported by Program of Higher-level Talents of Inner Mongolia University (30105-125136).

Notes and references

[a]*College of Chemistry and Chemical Engineering, Inner Mongolia University, Hohhot 010021, People's Republic of China.*
[b]*College of life science, Inner Mongolia University, Hohhot 010021, People's Republic of China.*
[c]*PhD school of materiaux, mechanics, environnement, energy, process and production engineering (I-MEP2), University of Grenoble, Grenoble 38031, France.*
[d]*College of Chemistry, Jilin University, Changchun 130021, People's Republic of China*

[1]*Contributed equally to this work.*

1 P. K. J. Robertson, J. M. C. Robertson and D. W. Bahnemann, *J. Hazard. Mater.*, 2012, **211-212**, 161.
2 J. Hewitt, G. E. Greening, M. Leonard and G. D. Lewis, *Water Res.*, 2013, **47**, 6750.
3 K. K. Schrader, F. Avolio, A. Andolfi, A. Cimmino and A. Evidente, *J. Agric. Food Chem.*, 2013, **61**, 1179.
4 S. C. Motshekga, S. S. Ray, M. S. Onyango and M. N. B. Momba, *J. Hazard. Mater.*, 2013, **262**, 439.
5 I. Ocsoy, M. L. Paret, M. A. Ocsoy, S. Kunwar, T. Chen, M. You and W. Tan, *ACS Nano*, 2013, **7**, 8972.
6 K. Yu, Y. Huang and S. Yang, *J. Hazard. Mater.*, 2013, **261**, 155.
7 I. Cerkez, H. B. Kocer, S. D. Worley, R. Broughton and T. S. Huang, *Cellulose*, 2012, **19**, 959.
8 E. Kenawy, S. D. Worley and R. Broughton, *Biomacromolecules*, 2007, **8**, 1359.
9 Z. Cao and Y. Sun, *ACS Appl. Mater. Interfaces*, 2009, **1**, 495.
10 F. Hui and C. Debiemme-Chouvy, *Biomacromolecules*, 2013, **14**, 585.
11 J. Lee, R. M. Broughton, A. Akdag, S. D. Worley and T. S. Huang, *Fiber. Polym.*, 2007, **18**, 148.
12 X. Ren, A. Akdag, C. Zhu, L. Kou, S. D. Worley and T.S. Huang, *J. Biomed. Mater. Res. Part A*, 2009, **91**, 385.
13 H. B. Kocer, S. D. Worley, R. M. Broughton and T. S. Huang, *React. Funct. Polym.*, 2011, **71**, 561.
14 Y. Sun and G. Sun, *J. Appl. Polym. Sci.*, 2003, **88**, 1032.
15 Y. Sun and G. Sun, *J. Polym. Sci.: Part A: Polym. Chem.*, 2001, **39**, 3348.
16 S. Liu and G. Sun, *Polymer*, 2008, **49**, 5225.
17 Z. Jie, X. Yan, L. Zhao, S. D. Worley and J. Liang, *React. Funct. Polym.*, 2013, **73**, 1580.
18 Z. Jie, X. Yan, L. Zhao, S. D. Worley and J. Liang, *RSC Adv.*, 2014, **4**, 6048.
19 Z. Kang, B. Zhang, Y. Jiao, Y. Xu, Q. He and J. Liang, *Cellulose*, 2013, **20**, 885.
20 K. Barnes, J. Liang, R. Wu, S. D. Worley, J. Lee, R. M. Broughton and T. S. Huang, *Biomaterials*, 2006, **27**, 4825.
21 E. O. Dorofeeva, M. N. Elinson, A. N. Vershchagin, N. O. Stepanov, I. S. Bushmarinov, P. A. Belyakov, O. O. Sokolova and G. I. Nikishin, *RSC Adv.*, 2012, **2**, 4444.
22 A. E. I. Ahmed, G. Cavalli, J. N. Wardell, M. E. Bushell and J. N. Hay, *Cellulose*, 2012, **19**, 209.
23 A. E. I. Ahmed, J. N. Hay, M. E. Bushell, J. N. Wardell and G. Cavalli, *J. Appl. Polym. Sci.*, 2010, **116**, 2396.
24 J. Jang and Y. Kim, *Chem. Commun.*, 2008, **34**, 4016.
25 S. Chen and W. Liu, *Langmuir*, 1999, **15**, 8100.
26 A. Dong, Q. Zhang, T. Wang, W. Wang, F. Liu and G. Gao, *J. Phys. Chem. C*, 2010, **114**, 17298.
27 A. Dong, J. Huang, S. Lan, T. Wang, L. Xiao. W. Wang, T. Zhao, X. Zheng, F. Liu, G. Gao and Y. Chen, *Nanotechnology*, 2011, **22**, 295602.
28 A. Dong, S. Lan, J. Huang, T. Wang, T. Zhao, W. Wang, L. Xiao, X. Zheng, F. Liu, G. Gao and Y. Chen, *J. Colloid Interface Sci.*, 2011, **364**, 333.
29 A. Dong, S. Lan, J. Huang, T. Wang, T. Zhao, L. Xiao, W. Wang, X. Zheng, F. Liu, G. Gao and Y. Chen, *ACS Appl. Mater. Interfaces*, 2011, **3**, 4228.
30 A. Dong, Y. Sun, S. Lan, Q. Wang, Q. Cai, X. Qi, Y. Zhang, G. Gao, F. Liu and C. Harnoode, *ACS Appl. Mater. Interfaces*, 2013, **5**, 8125.
31 A. Dong, Z. Huang, S. Lan, Q. Wang, S. Bao, Siriguleng, Y. Zhang, G. Gao, F. Liu and C. Harnoode, *J. Colloid Interface Sci.*, 2014, **413**, 92.
32 A. Dong, M. Xue, S. Lan, Q. Wang, Y. Zhao, Y. Wang, Y. Zhang, G. Gao, F. Liu and C. Harnoode, *Colloid. Surf. B*, 2014, **113**, 450.
33 Y. Sun and G. Sun, *J. Appl. Polym. Sci.*, 2001, **80**, 2460.
34 W. Wang, Y. Li, M. Sun, C. Zhou, Y. Zhang, Y. Li and Q. Yang, *Chem. Commun.*, 2012, **48**, 6040.
35 G. Yang, Y. Liu, R. Jia, R. Xu, X. Wang, L. Ling and J. Yang, *J. Appl. Polym. Sci.*, 2009, **112**, 410.
36 T. Don, S. Hsu and W. Chiu, *J. Polym. Sci. Part A*, 2001, **39**, 1646.
37 S. Lanners, H. Norouzi-Arasi, N. Khiri and G. Hanquet, *Eur. J. Org. Chem.*, 2007, 4065.
38 I. Ishikawa, V. E. Khachatrian, R. G. Melik-Ohanjanian, N. Kawahara, Y. Mizuno and H. Ogura, *Chem. Pharm. Bull.*, 1992, **40**, 846.
39 Z. Cao and Y. Sun, *J. Biomed. Mater. Res. Part A*, 2008, **85**, 99.
40 H. Lu, B. Xu, Y. Dong, F. Chen, Y. Li, Z. Li, J. He, H. Li and W. Tian, *Langmuir*, 2010, **26**, 6838-6844.
41 X. Huang, F. Hu and H. Su, *Macromolecules*, 2013, **46**, 1274.
42 U. Makal, L. Wood, D. E. Ohman and K. J. Wynne, *Biomaterials*, 2006, **27**, 1316.
43 W. Wang, Y. Zhang, Q. Yang, M. Sun, X. Fei, Y. Song, Y. Zhang and Y. Li, *Nanoscale*, 2013, **5**, 4958.
44 Z. Cao and Y. Sun, *Ind. Eng. Chem. Res.*, 2006, **45**, 2634.
45 W. Wang, X. Wang, Q. Yang, X. Fei, M. Sun and Y. Song, *Chem. Commun.*, 2013, **49**, 4833.
46 D. Wang, L. Xiao, Q. Luo, X. Li, J. An and Y. Duan, *J. Hazard. Mater.*, 2011, 192, 150.
47 V. Singh, A. K. Sharma, D. N. Tripathi and R. Sanghi, *J. Hazard. Mater.*, 2009, **161**, 955-966.
48 S. Li, Z. Li, K. N. Bozhilov, Z. Chen and Y. Yan, *J. Am. Chem Soc.*, 2004, **126**, 10732.
49 J. Ma, J. N. Wang and X. X. Wang, *J. Mater. Chem.*, 2009, **19**, 3033.
50 T. V. Khai, H. G. Na, D. S. Kwak, Y. J. Kwon, H. Ham, K. B. Shim and H. W. Kim, *J. Mater. Chem.*, 2012, **22**, 17992.
51 O. P. Khatri, T. Ichii, K. Murase, M. Kanehara, T. Teranishi and H. Sugimura, *J. Colloid Interface Sci.*, 2012, **382**, 22.
52 S. Zhou, L. Wang, Z. Lu, Q. Ding, S. C. Wang, R. J. K. Wood and Q. Xue, *J. Mater. Chem.*, 2012, **22**, 15782.
53 F. Amiri, M. M. F. Mesquita and S. A. Andrews, *Water Res.*, 2010, **44**, 845.
54 J. Luo, N. Porteous and Y. Sun, *ACS Appl. Mater. Interfaces*, 2011, **3**, 2895.
55 M. W. Eknoian, J. H. Putman and S. D. Worley, *Ind. Eng. Chem. Res.*, 1998, **37**, 2873.
56 S. Gokulajrishnan, P. Parakh and H. Praksash, *J. Hazard. Mater.*, 2012, **213-214**, 19.
57 C. Li, L. Xue, Q. Cai, S. Bao, T. Zhao, L. Xiao, G. Gao, C. Harnoode and A. Dong, *RSC Adv.*, 2014, **4**, 47853.
58 D. P. Tamboli and D. S. Lee, *J. Hazard. Mater.*, 2013, **260**, 878.
59 M. C. Rodríguez-Argüelles, C. Sieiro, R. Cao and L. Nasi, *J. Colloid Interface Sci.*, 2011, **364**, 80.

60 M. Omer-Mizrahi and S. Margel, *J. Colloid Interface Sci.*, 2009, **329**, 228.
61 Z. Cao and Y. Sun, *ACS Appl. Mater. Interfaces*, 2009, **1**, 494.
62 M. Braun and Y. Sun, *J. Polym. Sci. Part A: Polym. Chem.*, 2004, **42**, 3818.